

GRB 091208B: First Detection of the Optical Polarization in Early Forward Shock Emission of a Gamma-Ray Burst Afterglow

T. UEHARA¹, K. Toma², K. S. Kawabata³, S. Chiyonobu¹, Y. Fukazawa¹, Y. Ikejiri¹, T. Inoue⁴, R. Itoh¹, T. Komatsu¹, H. Miyamoto¹, T. Mizuno³, O. Nagae¹, H. Nakaya⁵, T. Ohsugi³, K. Sakimoto¹, M. Sasada¹, H. Tanaka¹, M. Uemura³, M. Yamanaka^{3,1}, T. Yamashita⁴, R. Yamazaki⁴, M. Yoshida³

ABSTRACT

We report that the optical polarization in the afterglow of GRB 091208B is measured at $t = 149 - 706$ s after the burst trigger, and the polarization degree is $P = 10.4\% \pm 2.5\%$. The optical light curve at this time shows a power-law decay with index -0.75 ± 0.02 , which is interpreted as the forward shock synchrotron emission, and thus this is the first detection of the early-time optical polarization in the forward shock (rather than that in the reverse shock reported by Steele et al. (2009)). This detection disfavors the afterglow model in which the magnetic fields in the emission region are random on the plasma skin depth scales, such as amplified by the plasma instabilities, e.g., Weibel instability. We suggest that the fields are amplified by the magnetohydrodynamic instabilities, which would be tested by future observations of the temporal changes of the polarization degrees and angles for other bursts.

Subject headings: gamma-ray burst: individual (GRB 091208B) – polarization – shock waves – magnetic fields

¹Department of Physical Science, Hiroshima University, Kagamiyama 1-3-1, Higashi-Hiroshima 739-8526, Japan; uehara@hep01.hepl.hiroshima-u.ac.jp

²Department of Earth and Space Science, Osaka University, Toyonaka 560-0043, Japan

³Hiroshima Astrophysical Science Center, Hiroshima University, Higashi-Hiroshima, Hiroshima 739-8526, Japan

⁴Department of Physics and Mathematics, Aoyama Gakuin University, Fuchinobe, Chuou-ku, Sagami-hara 252-5258, Japan

⁵National Astronomical Observatory of Japan, Osawa, Mitaka, Tokyo 181-8588, Japan

1. Introduction

Many of the gamma-ray burst (GRB) afterglows can be explained as the synchrotron emission from the shock produced by the interaction of the ejecta with the circumburst medium (Zhang & Mészáros 2004; Piran 2004, for reviews), and their spectra and light curves have helped us understand the total energy scale, the outflow structure, and the circumburst medium profile as well as the micro-physical conditions of the relativistic collisionless shock for each afterglow (e.g., Panaitescu & Kumar 2002).

Major problems on the physics of the relativistic collisionless shocks involve how to accelerate particles into the population with the power-law energy distribution $dn/d\gamma \propto \gamma^{-p}$, where γ is the electron Lorentz factor, and how to amplify the magnetic field from the typical strength in the interstellar medium $\sim 1 \mu\text{G}$ to the strength required to produce bright synchrotron radiation $\sim 1 \text{ G}$ for GRB afterglows. Polarimetric observations of synchrotron radiation from the relativistic shocks can reveal the magnetic field structure. The field structure is essential for constraining the mechanisms of field amplification and particle acceleration (see also Toma, Ioka, & Nakamura 2008). The extensive polarimetric observations of the late-time optical afterglows ($t \sim 1 \text{ day}$) have been performed (Covino et al. 2004),¹ although the field structure is still in debate (for a review, see Lazzati 2006). Early polarimetric observation is crucial.

Polarimetric observation generally needs large amount of photons and therefore needs a larger telescope than typical imaging, because the required accuracy is mostly of $\leq 1\%$ order. To obtain polarimetric data of early afterglow of GRBs, we should have a polarimeter of which the field of view is larger than the initial position error of GRBs ($\sim 3'$) as well as a quickly-moving telescope. Since the early emission of GRBs changes rapidly, the polarimeter should also have a function to obtain all Stokes parameters for linear polarization, I , Q , and U within a short timescale.

Recently, optical polarimetry has been performed at the early phase. Mundell et al. (2007) reported an upper limit on the polarization degree of GRB 060218 as $P < 8\%$ at $t \gtrsim 203 \text{ s}$, corresponding to the onset phase of the forward shock. Steele et al. (2009) detected an optical polarization of $P = 10\% \pm 1\%$ at $t \gtrsim 161 \text{ s}$ in the reverse shock emission of GRB 090102. Both GRBs were observed by RINGO attached to the 2.0-m robotic Liverpool Telescope, which uses a rotating polarizer that is recoded on a CCD.

In this Letter, we report the first detection of the early forward shock optical polarization for GRB 091208B with the Kanata 1.5 m telescope at Higashi-Hiroshima Observatory. The optical emission is explained as the forward shock synchrotron emission, and the polarization degree is $P = 10.4\% \pm 2.5\%$ averaged over $t = 149 - 706 \text{ s}$. The polarization of the forward shock emission

¹ Here and hereafter we define t as the time after the burst trigger.

provides us with the information on the structure of the magnetic field amplified from the weak circumburst magnetic field, rather than possible magnetic fields advected from the central engine which may be probed with the polarization from the reverse shock (Steele et al. 2009). It also might be interesting to compare our data for the optical afterglow with the recent claim of detection of γ -ray polarization $P_\gamma = 27\% \pm 11\%$ in the prompt emission of GRB 100826A (Yonetoku et al. 2011).

The prompt emission of GRB 091208B has the duration $T_{90} = 14.9 \pm 3.7$ s, and the fluence in the 15–150 keV band $f_\gamma = (3.3 \pm 0.2) \times 10^{-6}$ erg cm⁻². The redshift is determined as $z \simeq 1.063$, so that the isotropic γ -ray energy is estimated as $E_{\gamma,\text{iso}} \simeq 1 \times 10^{52}$ erg (Pagani et al. 2010).

2. Optical Data: Observations and Reduction

We performed optical imaging polarimetry of GRB 091208B with HOWPol (Hiroshima One-shot Wide-field Polarimeter; Kawabata et al. 2008) attached to the Nasmyth focus on 1.5-m Kanata telescope at Higashi-Hiroshima Observatory, Japan. Since HOWPol uses a wedged double Wollaston prism (Oliva 1997) at the pupil image position after the collimator lens, four images by linearly polarized rays at 0°, 90°, 45° and 135° position angles (PAs), respectively, are recorded on two 2k4k HPK CCDs simultaneously. This enables us to obtain all three Stokes parameters for linear polarization, i.e., I , Q , U , from only a single exposure. Our observation started at 2009 Dec 8.41142 UT, $t = 149$ s, which was automatically processed after receiving the *Swift*/BAT Notice via GCN. This is one of the earliest polarimetry to date, as far as we know. We took ten 30 s exposures and then nine 60 s exposures through a $15'\phi$ aperture mask and an R -band filter. The observation finished at Dec 8.42458, $t = 1286$ s. Figure 1 shows a sample image of GRB 091208B obtained with HOWPol.

The raw data were reduced in a standard way for CCD aperture photometry. For the photometric calibration, we used $R2$ magnitudes of three nearby stars (C1–C3: USNO B 1068-0020023, 1068-0020019, and 1069-0020340). The optical light curve can be described with a single power-law form (decay index $\alpha_O = -0.75 \pm 0.02$), as shown in Figure 2. For polarimetry, we could not use the sixth exposure (centered at $t = 376$ s) and all exposures after 13th ($t = 791$ s) because one polarization image of the GRB out of four falls into the gap of the two CCDs due to slight telescope guiding error. It reduces the number of the available frames for polarimetry to 11. As for polarimetric calibration, we corrected for the instrumental polarization of $P_{\text{instr}} \simeq 3.9\%$, predominantly caused by the 45°-incidence reflection on the tertiary mirror of the telescope. The instrumental polarization has been modeled with an accuracy of $\Delta P_{\text{instr}} \lesssim 0.5\%$ as a function of the hour angle and the declination (and also of the position taken in the field of view) of the object by systematic observations for unpolarized standard stars, and then checked by observations for strongly-polarized

standard stars. In the case of GRB 091208B, it changed gradually with time from $Q_{\text{instr}} = -3.65$ % to -3.70 % and $U_{\text{instr}} = -1.05$ % to -0.88 % over the 11 exposures. The detailed procedure and reliability of this ‘one-shot polarimetry’ will appear in a forthcoming paper (Kawabata K. S., et al., in preparation).

Since the S/N ratio of each single exposure is not sufficient for polarimetry ($\Delta P \gtrsim 5$ %), we combined the all 11 Q and U parameters to enhance the reliability. We performed a traditional, statistic correction for the polarization bias in cases of low S/N as $P_{\text{real}} = \sqrt{P^2 - (\sigma_P)^2}$ (Serkowski 1958, see also Patat & Romaniello 2006). The derived polarization is $Q = -10.3\% \pm 2.5\%$, $U = -0.7\% \pm 2.2$ % (i.e., $P = 10.4\% \pm 2.5$ %, $\text{PA} = 92^\circ \pm 6^\circ$). The Galactic interstellar extinction indicates that the interstellar polarization toward this GRB is negligibly small ($P_{\text{ISP}} \leq 9E_{B-V} = 0.5$ % ; Serkowski, Mathewson, & Ford 1975; Schlegel, Finkbeiner, & Davis 1998). To check the consistency, we obtained the polarization of nearby stars ($\leq 4'$) brighter than or comparably faint to the GRB a fterglow taken in the same frames, and plot them in QU -diagram (Figure 3). Assumed that they are mostly Galactic normal stars having little or no intrinsic polarization, the diagram would support that the GRB afterglow has a significant polarization.

3. X-ray Data: Reduction and Analysis

We reduced the public data of XRT on *Swift* for GRB 091208B, using the XRT pipeline FTOOL *xrtpipeline* (Version: 2.3.3). The obtained 0.3–10 keV light curve is shown in Figure 2. The first orbit data at $t = 130$ –600s exhibits possible bumps and mini-flares (cf. Pagani et al. 2010). The following orbit data can be described with a broken power-law form; $F_\nu \propto t^{\alpha_{X,2}} (t \leq t_{X,\text{break}})$ and $F_\nu \propto t^{\alpha_{X,3}} (t > t_{X,\text{break}})$. We obtained the decay indices and the break time as listed in Table 1.

Based on the variability in the light curve, we defined three phases for GRB 091208B, as described in Table 1. For each phase, we obtained the time-averaged spectrum at 0.3–8.0 keV. We fitted a power-law model having two absorption components to the X-ray data. One component is the absorption in our galaxy and the other is the host galaxy. For the former, the Galactic hydrogen column density has been derived as $N_{\text{H}}^{\text{gal}} = 4.8 \times 10^{20} \text{ cm}^{-2}$ for the direction of GRB 091208B (Schlegel, Finkbeiner, & Davis 1998; Dickey & Lockman 1990) and we fixed it. For the latter, we confirmed that the column density in the host galaxy $N_{\text{H}}^{\text{ext}}$ is practically constant by our trial fitting and put $N_{\text{H}}^{\text{ext}}$ as a common parameter for all three phases. We show the result of our fitting in Table 1. $N_{\text{H}}^{\text{ext}}$ is derived as $(8.0 \pm 2.1) \times 10^{21} \text{ cm}^{-2}$. It is noted that the spectral index β_X does not significantly change through the period of our optical polarimetry.

In Figure 4, we show the spectral energy distribution (SED) from optical (3.9×10^{14} Hz) to X-ray band (1.1×10^{18} Hz) at $t = 162$ –589 s. The Galactic extinction of $E_{B-V} = 0.162$ (Schlegel, Finkbeiner, & Davis

1998) has been corrected for using a standard way. On the other hand, for the extinction within the host galaxy, we adopted three extinction curve models, the Milky Way (MW), the Large Magellanic Cloud (LMC), and the Small Magellanic Cloud (SMC) models, while the hydrogen column density ($N_{\text{H}}^{\text{ext}} = 8.0 \times 10^{21} \text{ cm}^{-2}$) is fixed (Uehara et al. 2010, 2011). Using one of these 3 models, we corrected the extinction in the optical bands. The extinction for the SMC model (or less than that) seems reasonable, since the temporal decay of the optical flux implies a soft spectrum in the synchrotron model. In this case, the flux density is $1.4 \pm 0.3 \text{ mJy}$ at $3.9 \times 10^{14} \text{ Hz}$.

4. Discussion

4.1. Modeling of the afterglow

The observed optical afterglow has a typical power-law light curve that is explained by the synchrotron emission from the forward shock propagating in the external medium (Meszaros & Rees 1997; Sari, Piran, & Narayan 1998). The decay index $\alpha_{\text{O}} = -0.75 \pm 0.02$ is very likely to be the case $\nu_m < \nu_{\text{O}} < \nu_c$ with the uniform-density external medium and $p \simeq 2.0$, where $\nu_{\text{O}} \equiv 3.9 \times 10^{14} \text{ Hz}$, ν_m is the minimum injection frequency, ν_c is the cooling frequency, and p is the index of the electron energy distribution (see Table 1 of Zhang & Mészáros 2004). The X-ray emission in the second phase also looks a typical power-law light curve, although we find that the above model for the optical emission cannot explain the X-ray emission simultaneously, as shown below.

The X-ray emission in the second phase shows $\alpha_{\text{X},2} - 3\beta_{\text{X},2}/2 = 0.48 \pm 0.24$. This can be interpreted as the case $\nu_{\text{X}} > \max(\nu_m, \nu_c)$ with $p \sim 2.1$. Thus one may consider the case $\nu_m < \nu_{\text{O}} < \nu_c < \nu_{\text{X}}$ in this phase. At some time earlier, $\nu_c (\propto t^{-1/2})$ may have passed across ν_{X} , which means that the X-ray light curve can have a break and the decay index before the break is the same as α_{O} . This enables us to have an X-ray light curve that is not brighter than the observed X-ray emission in the first phase. In this case, however, the optical and X-ray synchrotron emissions are in the same spectral segment, i.e., $\nu_m < \nu_{\text{O}} < \nu_{\text{X}} < \nu_c$ with $\beta_{\text{O}} = \beta_{\text{X}} \simeq -(p-1)/2 \sim -0.55$, which is not compatible with the observed joint spectrum in Figure 4, in which the blue line has the spectral index -0.72 ± 0.01 . The extrapolation of the optical flux at the higher frequencies with such a value of β_{O} overwhelms the observed X-ray flux.

Considering that the observed X-rays at the first phase shows several flares, it is reasonable that the optical emission is the forward shock synchrotron radiation with $\nu_m < \nu_{\text{O}} < \nu_c$, whereas the X-ray emission has different origins. Many models have been proposed for such anomalous X-ray afterglows (e.g., Ghisellini et al. 2007; Kumar, Narayan & Johnson 2008; Yamazaki 2009). In this case, the extrapolation of the optical flux at the higher frequencies has to have a cooling break at $\nu_{\text{O}} < \nu_c (t \sim 300 \text{ s}) \lesssim 10^{16} \text{ Hz}$ to suppress the emission below the observed X-rays. The other

necessary conditions for this model are the following: $\nu_m(t \sim 80 \text{ s}) < \nu_0$ and $\nu_c(t \sim 5 \times 10^4 \text{ s}) \gtrsim \nu_0$ to have a single power-law light curve at the optical band; and $F_O(t \sim 300 \text{ s}) \simeq 1 \text{ mJy}$. The condition for ν_c can be summarized by using $\nu_c \propto t^{-1/2}$ as $5.0 \times 10^{15} \text{ Hz} \lesssim \nu_c(t \sim 300 \text{ s}) \lesssim 10^{16} \text{ Hz}$.

The characteristic quantities in the forward shock synchrotron model with the uniform-density external medium are given by Granot & Sari (2002)

$$\nu_m \simeq 7.1 \times 10^{10} E_{52}^{1/2} \epsilon_{e,-1}^2 f_{-1}^2 \epsilon_{B,-2}^{1/2} t_{\text{days}}^{-3/2} \text{ Hz}, \quad (1)$$

$$\nu_c \simeq 6.7 \times 10^{15} E_{52}^{-1/2} \epsilon_{B,-2}^{-3/2} n_0^{-1} t_{\text{days}}^{-1/2} \text{ Hz}, \quad (2)$$

$$F_{\nu_m} \simeq 0.91 E_{52} \epsilon_{B,-2}^{1/2} n_0^{1/2} \text{ mJy}, \quad (3)$$

where $E_{\text{iso}} = 10^{52} E_{52} \text{ erg}$ is the total isotropic energy of the blast wave, which may be comparable to $E_{\gamma, \text{iso}} \simeq 1 \times 10^{52} \text{ erg}$ (see Section 1), $n = 1 n_0 \text{ cm}^{-3}$ is the density of the external medium, $\epsilon_e = 10^{-1} \epsilon_{e,-1}$ and $\epsilon_B = 10^{-2} \epsilon_{B,-2}$ are the fractions of the shocked energy carried by the electrons and the magnetic field, respectively. The case of $p \simeq 2.0$ involves the factor $f = 1 / \ln(\gamma_M / \gamma_m)$, where γ_M and γ_m are the maximum and minimum injection Lorentz factors of electrons, respectively, and f typically has a value of $\sim 10^{-1}$. The optical emission is calculated as $F_O = F_{\nu_m} (\nu_O / \nu_m)^{-(p-1)/2}$. The necessary conditions given above are translated into

$$E_{52}^{1/2} \epsilon_{e,-1}^2 f_{-1}^2 \epsilon_{B,-2}^{1/2} < 0.15, \quad (4)$$

$$E_{52}^{1/2} \epsilon_{B,-2}^{3/2} n_0 \simeq 11.4 y, \quad (5)$$

$$E_{52}^{5/4} \epsilon_{B,-2}^{3/4} \epsilon_{e,-1} f_{-1} n_0^{1/2} \simeq 1.2, \quad (6)$$

where we define a numerical factor $1 \lesssim y \lesssim 2$. The equations are reduced into $\epsilon_{e,-1} f_{-1} \simeq 0.35 E_{52}^{-1} y^{-1/2}$, $\epsilon_{B,-2} < 1.6 E_{52}^3 y^2$, and $n_0 > 5.5 E_{52}^{-5} y^{-3}$. These equations indicate that the optical emission can be understood as the forward shock synchrotron emission with the typical parameter values (Panaitescu & Kumar 2002).

4.2. Implications from optical polarization

We have measured the optical polarization in the early forward shock emission of this burst as $P = 10.4\% \pm 2.5\%$. Since this is a mean value over a long observation time $t = 149 - 706 \text{ s}$, the actual polarization degree might have been either unusually constant or temporally much higher. This result disfavors the afterglow model in which the magnetic field coherent scales are plasma skin depths in the emission region, as explained below.

The magnetic field can be amplified by the plasma instabilities at the shock front, such as Weibel instability. This can produce the strong fields with random directions on the skin

depth scales, which are very tiny compared with the size of the observable region of the shock (Medvedev & Loeb 1999). The field directions are possibly constrained to be parallel to the shock plane. In this case, however, the observed polarization reaches a maximum value around the jet break time (typically around $t \sim 1$ day) in general (Sari 1999; Ghisellini & Lazzati 1999; Rossi et al. 2004). Our measurement of the early optical polarization which is higher than the typical late-time polarization, $\sim 1\text{--}3\%$ (at $t \sim 1$ day; Covino et al. 2004) is thus not consistent with this mechanism.² Some polarization angle data at late-time are also incompatible with this mechanism (Lazzati et al. 2004; Lazzati 2006). Furthermore, the numerical simulations of collisionless shocks suggest that the fields produced by the plasma instabilities decay fast and do not survive on the large scales corresponding to the emission region (Sironi & Spitkovsky 2009; Gruzinov & Waxman 1999).

We suggest that magnetohydrodynamic (MHD) instabilities may be viable for the magnetic field origin in the emission region, rather than the plasma instabilities. If the shock sweeps inhomogeneous external medium, multiple vorticities arise downstream of the shock due to the growth of the Richtmyer-Meshkov instability, increasing the field strength (Sironi & Goodman 2007; Inoue, Asano & Ioka 2011). The numerical simulations show that this mechanism can produce strong fields random on large scales that are roughly comparable to the density fluctuation scale of the external medium. Such large-scale fields decay rather slowly, which may survive in the entire emission region. In this case the observed polarization scales as $P \sim 70\% / \sqrt{N}$, where N is the number of the coherent field patches in the observable region $\theta \lesssim 1/\Gamma$ (Gruzinov & Waxman 1999). Our measured polarization degree means $N \sim 50(P/10\%)^{-2}$. Since the radius R and the Lorentz factor Γ of the forward shock are estimated to be $R \simeq 4.6 \times 10^{17} E_{52}^{1/4} n_0^{-1/4} t_{\text{days}}^{1/4}$ cm, and $\Gamma \simeq 4.7 E_{52}^{1/8} n_0^{-1/4} t_{\text{days}}^{-3/8}$ (Granot & Sari 2002), we may estimate the typical scale of the field coherent patch at $t \sim 300$ s as $l_p \sim (R/\Gamma) / \sqrt{N} \sim 4 \times 10^{14} E_{52}^{1/8} n_0^{-1/8} (P/10\%)$ cm. The coherent patches with such scales might be formed by the density fluctuations in molecular cloud cores or HI clouds in the interstellar medium, of which the sizes are typically $\sim 10^{16} - 10^{17}$ cm.

In this model, the polarization angle randomly changes with time, and the polarization degree scales as

$$P \propto 1/\sqrt{N} \propto l_p (R/\Gamma)^{-1} \propto l_p E^{-1/8} n^{1/8} t^{-5/8}. \quad (7)$$

At $t \sim 1$ day, this burst may show $P \sim 0.3\%$, if l_p is roughly constant through the shock propagation. This value is comparable to (or somewhat smaller than) the typical late-time polarization, $\sim 1\text{--}3\%$. If the shock propagates in the magnetized wind from the progenitor star, the polarization from the

²The jet with non-uniform angular energy distribution and with the plasma-scale fields can produce high degree of polarization at any times (Nakar & Oren 2004), although it may not produce such a smooth light curve as we observed. The residuals of our optical data at $t = 149 - 706$ s from the power-law model are all within the 1σ level.

ordered field, which has roughly constant degree and angle, contributes to the net polarization (Granot & Königl 2003), although the light curve of this burst implies that the density profile of the external medium is constant ($n \propto r^0$) rather than the wind type ($n \propto r^{-2}$) (see Section 4.1).

The result of Mundell et al. (2007), a 2σ upper-limit $P < 8\%$ for GRB 060418, might imply that l_p was several times smaller than that for the GRB 091208B case. Anyway, we need more data of polarization and also their time variation for other bursts, which would further constrain the field structure in the emission region and the nature of the environment of GRBs.

This work is supported by JSPS Research Fellowships for Young Scientists (TU, KT, RI, MS, MY) and by the Grant-in-Aid for Scientific Research from JSPS (17684004, 19047003, 23244030, 23340048, 60372702).

REFERENCES

- Covino, S., Ghisellini, G., Lazzati, D., & Malesani, D. 2004, in ASP Conf. Ser. 312, Third Rome Workshop on Gamma-Ray Bursts in the Afterglow Era, eds. M. Feroci, F. Frontera, N. Masetti, & L. Piro (San Francisco: ASP), 169
- Dickey, J. M., & Lockman, F. J. 1990, ARA&A, 28, 215
- Ghisellini, G., & Lazzati, D. 1999, MNRAS, 309, L7
- Ghisellini, G., Ghirlanda, G., Nava, L., & Firmani, C. 2007, ApJ, 658, L75
- Granot, J., & Königl, A. 2003, ApJ, 594, L83
- Granot, J., & Sari, R. 2002, 568, 820
- Gruzinov, A., & Waxman, E. 1999, ApJ, 511, 852
- Inoue, T., Asano, K., & Ioka K. 2011, ApJ, 734, 77
- Kawabata, K. S., Nagae, O., Chiyonobu, S., et al. 2008, Proc. SPIE, 70144L
- Kumar, P., Narayan, R., & Johnson, J. L. 2008, MNRAS, 388, 1729
- Lazzati, D. 2006, New Journal of Physics, 8, 131
- Lazzati, S., et al. 2004, A&A, 422, 121
- Medvedev, M. V., & Loeb, A. 1999, ApJ, 526, 697

- Meszáros, P., & Rees, M. J. 1997, *ApJ*, 476, 232
- Mundell, C. G., Steele, I. A., Smith, R. J., et al. 2007, *Science*, 315, 1822
- Nakar, E., & Oren, Y. 2004, *ApJ*, 602, L97
- Oliva, E. 1997, *A&AS*, 123, 589
- Pagani, C., de Pasquale, M., & Baumgartner, W. H. 2010, *GCN Rep.*, 266, 1
- Panaitescu, A., & Kumar, P. 2002, 571, 779
- Patat, F., & Romaniello, M. 2006, *PASP*, 118, 146
- Piran, T. 2004, *Rev. Mod. Phys.*, 76, 1143
- Rossi, E. M., Lazzati, D., Salmonson, J. D., & Ghisellini, G. 2004, *MNRAS*, 354, 86
- Sari, R. 1999, *ApJ*, 524, L43
- Sari, R., Piran, T., & Narayan, R. 1998, *ApJ*, 497, L17
- Schlegel, D. J., Finkbeiner, D. P., & Davis, M. 1998, *ApJ*, 500, 525
- Serkowski, K. 1958, *Acta Astron.*, 8, 135
- Serkowski, K., Mathewson, D. S., & Ford, V. L. 1975, *ApJ*, 196, 261
- Sironi, L., & Goodman, J. 2007, *ApJ*, 671, 1858
- Sironi, L., & Spitkovsky, A. 2009, *ApJ*, 698, 1523
- Steele, I. A., Mundell, C. G., Smith, R. J., Kobayashi, S., & Guidorzi, C. 2009, *Nature*, 462, 767
- Toma, K., Ioka, K., & Nakamura, T. 2008, *ApJ*, 673, L123
- Uehara, T., Uemura, M., Kawabata, K. S., et al. 2010, *A&A*, 519, A56
- Uehara, T., Uemura, M., Arai, A., et al. 2011, *A&A*, 526, A92
- Yamazaki, R. 2009, *ApJ*, 690, L118
- Yonetoku, D., Murakami, T., Gunji, S., et al. 2011, *ApJ*, 743, L30
- Zhang, B., & Mészáros, P. 2004, *International Journal of Modern Phys. A*, 19, 2385

Table 1: Decay and spectral indices of the X-ray afterglow of GRB 091208B

Phase	T (s)	α_X^\dagger	β_X^\ddagger
<i>First</i>	130–600	-0.18 ± 0.15	-0.97 ± 0.14
<i>Second</i>	$5300-3.1 \times 10^5$	-1.10 ± 0.12	$-1.05^{+0.14}_{-0.13}$
<i>Third</i>	$3.1 \times 10^5-1.0 \times 10^6$	$-2.3^{+1.6}_{-1.2}$	$-0.82^{+0.30}_{-0.42}$

The uncertainties show the 90% confidence levels of the parameters.

\dagger X-ray decay index.

\ddagger X-ray spectral index ($\chi^2/\text{d.o.f} = 60.9/78$).

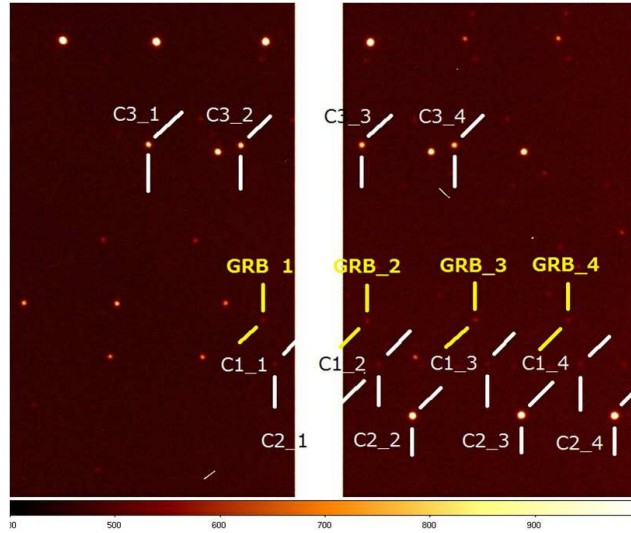


Fig. 1.— A sample image obtained by HOWPol in one-shot polarimetry mode for GRB 091208B. Each object produces four images by linearly polarized rays at 0° , 90° , 45° and 135° position angles, respectively, on the projected sky. C1–C3 are comparison stars for the magnitude reference. The vertical gap around the center ($\sim 40''$ width) is due to the mechanical gap between the two CCDs.

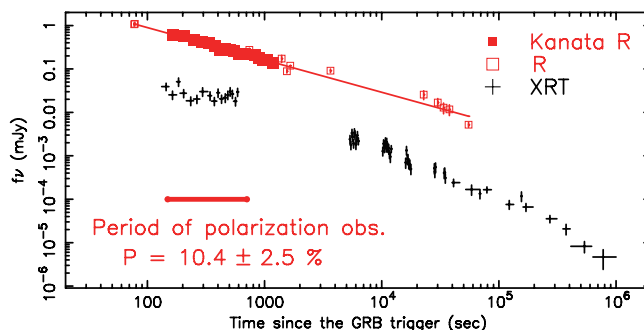


Fig. 2.— Optical and X-ray light curves of GRB 091208B. Our optical and *Swift*/XRT data are indicated by the filled squares and crosses, respectively. Open squares are the optical data reported in GCN. The solid lines are the best fitted power-law models for the optical light curve (with the decay index of $\alpha_0 = -0.75 \pm 0.02$). The thick horizontal bar at the left bottom part shows the period of our polarimetry. The derived polarization degree is also indicated.

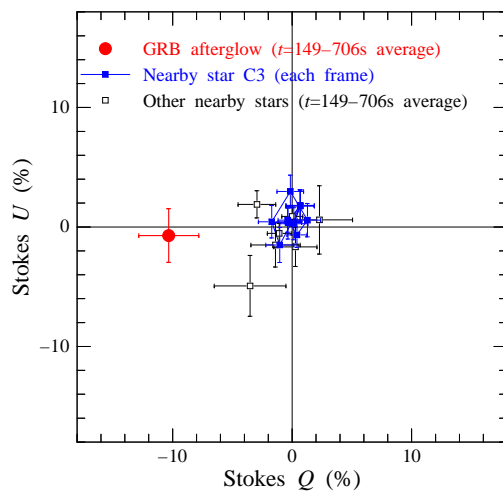


Fig. 3.— QU -diagram of the GRB afterglow and nearby stars. For the bright comparison star C3, we demonstrate the frame-to-frame variation of Q and U , which suggests the residual systematic is negligible ($\lesssim 1\%$). For other stars we show time-averaged polarization at $t = 149 - 706$ s.

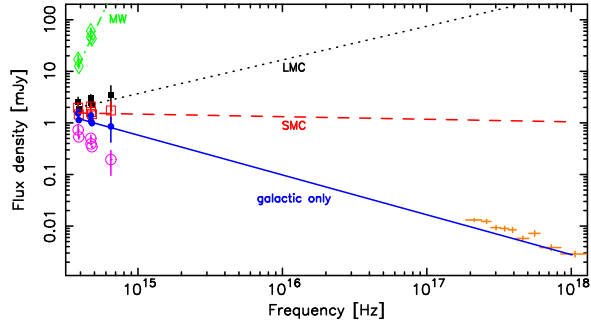


Fig. 4.— SED of the Optical – X-ray regime of GRB 091208B on $t = 162 - 589$ s. The crosses show the unabsorbed X-ray spectra. The purple open circles are raw optical data, and the blue small filled circles are optical ones dereddened for the Galactic extinction only ($E_{B-V} = 0.162$). The red open squares, black filled squares and green open squares are optical data dereddened for the host extinction ($N_{\text{H}}^{\text{ext}} = 8.0 \times 10^{21} \text{ cm}^{-2}$) of the SMC, LMC and MW models, respectively, in addition to the Galactic extinction. The blue solid, red dashed, black dotted, and green dashed-dotted lines indicate the best-fitted power-law models of the individual dereddened optical data. The blue solid line (with power-law index $\beta = -0.72 \pm 0.01$) appears consistent with the X-ray data, too; however, this spectral model is not compatible with the temporal evolutions of the optical and X-ray fluxes in the forward shock synchrotron model (see § 4.1).